



UNIVERSITY OF LEEDS

This is a repository copy of *Assessment and Retrofitting of an Existing Steel Structure subjected to Wind-Induced Failure Analysis*.

White Rose Research Online URL for this paper:
<http://eprints.whiterose.ac.uk/140614/>

Version: Accepted Version

Article:

Maraveas, C and Tsavdaridis, KD orcid.org/0000-0001-8349-3979 (2019) Assessment and Retrofitting of an Existing Steel Structure subjected to Wind-Induced Failure Analysis. *Journal of Building Engineering*, 23. pp. 53-67. ISSN 2352-7102

<https://doi.org/10.1016/j.jobe.2019.01.005>

© 2019 Elsevier Ltd. This manuscript version is made available under the CC-BY-NC-ND 4.0 license <http://creativecommons.org/licenses/by-nc-nd/4.0/>.

Reuse

This article is distributed under the terms of the Creative Commons Attribution-NonCommercial-NoDerivs (CC BY-NC-ND) licence. This licence only allows you to download this work and share it with others as long as you credit the authors, but you can't change the article in any way or use it commercially. More information and the full terms of the licence here: <https://creativecommons.org/licenses/>

Takedown

If you consider content in White Rose Research Online to be in breach of UK law, please notify us by emailing eprints@whiterose.ac.uk including the URL of the record and the reason for the withdrawal request.



eprints@whiterose.ac.uk
<https://eprints.whiterose.ac.uk/>

Assessment and Retrofitting of an Existing Steel Structure subjected to Wind-Induced Failure Analysis

C. Maraveas^{1,2*} and K.D. Tsavdaridis³

¹C. MARAVEAS & ASSOCIATES P.C. - Consulting Engineers, Greece

²Fire Safety Unit, ArGenCo Dept., University of Liege, Belgium

³School of Civil Engineering, University of Leeds, UK

*Corresponding author. E-mail address: c.maraveas@maraveas.gr

Abstract

Wind loads are a major threat for old corroded steel structures constructed near the sea where wind speeds can be very high. This paper presents a case study of a wind-induced failure analysis of an existing steel structure and the proposed retrofitting methods. The examined steel structure was constructed in the 1970s in Syros, Greece and is currently operating as an athletic centre. The first part of this study presents the wind-induced failure analysis, from which a domino effect is documented. A corroded bracing that was buckled due to wind load governs the reduction of vertical load carrying of the steel structure and creates an asymmetry under horizontal loading before a number of other steel members failed due to buckling. To understand the structure's performance, failure analysis, as well as time history and incremental dynamic analysis, were performed. The second part of this paper presents the proposed retrofitting methods for improving the vertical load carrying capacity under wind loads. The goal was to improve the load-carrying capacity of the structure so as to comply with current design European codes. In addition, enhancement of the dynamic properties of the strengthened structure was demonstrated using modal analyses. The structural behaviour was determined in a more precise manner via non-linear wind time-history and incremental static analyses. The analytical results explain the development of failures in the existing structure.

Keywords: wind-induced analysis, steel buckling, structural assessment, strengthening, rehabilitation, repair, time-history analysis, incremental static analysis, modal analysis.

1. Introduction

Safety concern is a challenge when dealing with damaged existing structures of high importance which are also currently in use. The two main goals of structural assessment for existing structures are to predict adequate structural behaviour (and thus satisfying reliability throughout its service life) and to optimize cost [1].

To the best of the authors' knowledge, most researchers, thus far, have addressed wind engineering at a theoretical level [2-6] without coupling their analyses with case-study failure investigations. Some studies have used database-assisted or testing-assisted design methodologies [2-4], while wind loading simulations performed via stochastic processes have drawn significant interest over the past few decades [5-8]. Wind loads are critical for tall buildings [9], but also for low-rise structures [10-12] similar to this study.

The field of forensic structural engineering has also become attractive recently for many engineers around the world. Ratay published an overview [13], in which the main aspects, difficulties, and future dynamics of wind-failure forensic fields are presented. Structural failure is typically defined as non-conformant with design expectations that provide minimum performance requirements. However, it can also consist of a high risk of potential failure. There are typically no signs of deterioration in the latter case. Conclusions can be determined via structural analyses or/and field investigation and testing. Moreover, the author highlights individual skills and judgment and even the temperament of the specialist-engineer, as being of major importance.

The present work addresses a case-study of a steel structure with significant enough damage to "threaten" its safety. Strengthening measures are thought to be necessary in order to protect human life. The paper also focuses on the precise response of the structure under realistic simulations of environmental actions, in particular, wind actions.

The "Dimitrios Vikelas" athletic centre in Ermoupolis of Syros (Greece) is selected and it consists of two buildings. Building B has a steel superstructure that was constructed approximately 35 years ago. It was initially used as a boat shelter and no design calculations were available, possibly constructed as a pre-engineered structure. It contains steel columns with varying cross-section heights. The spans are bridged via trusses and I-beams. Significant geometrical inconsistencies are noted among the existing steel connections and failures have been resulted due to buckling in several beams and bracings during the service life of the athletic centre. The current study presents an investigation performed in order to diagnose structural problems and propose strengthening and intervention measures.

The overall plan area of the metal building is 1228 m². It has a rectangular layout with dimensions of 33.0 m by 36.0 m between the column axes and a roof height that varies from +8.24 m to +12.12 m from ground level. The structure consists of 7 parallel frames spaced at equal distances of 6.0 m. Each frame consists of two parts: the southernmost part includes 560/170x170mm (H type) steel columns of varying web heights and an IPE270 frame rafter with a 7.21 m clear opening, while the northernmost part includes 690/190x190mm (H type) steel columns of varying web heights. The 24.8 m opening in the latter part is bridged via trusses from double angle sections for the chords and single angle sections for the web (all connected through welded connections), as presented in Fig. 2. In the middle, the two parts are supported on IPE360 steel columns.

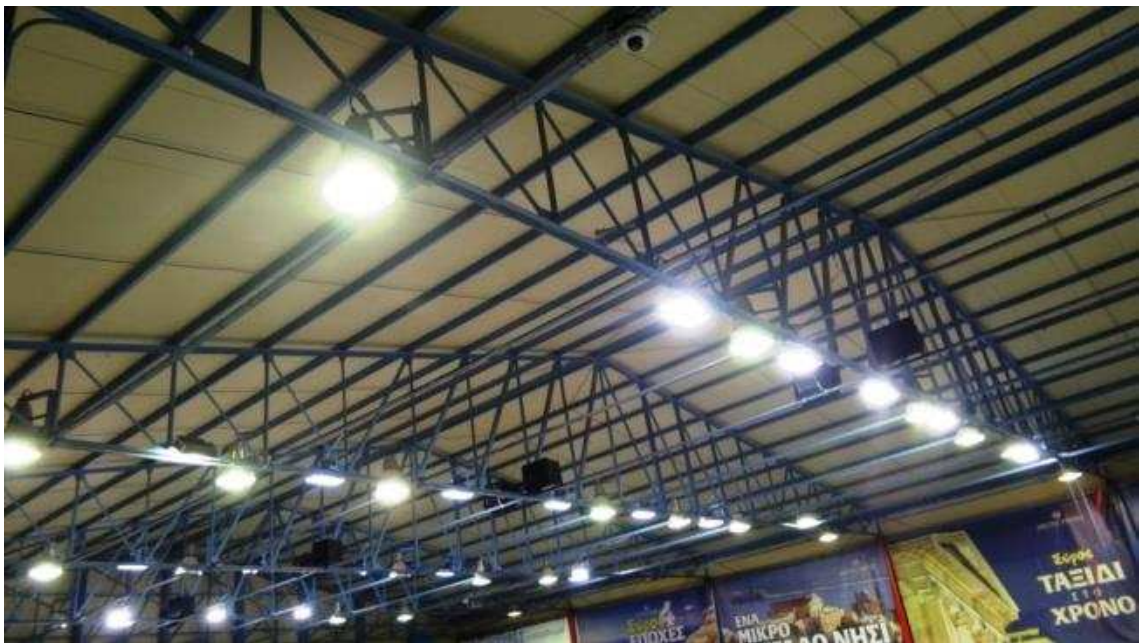


a)



b)

Fig. 1. Views of the a) west and b) east sides of the building.



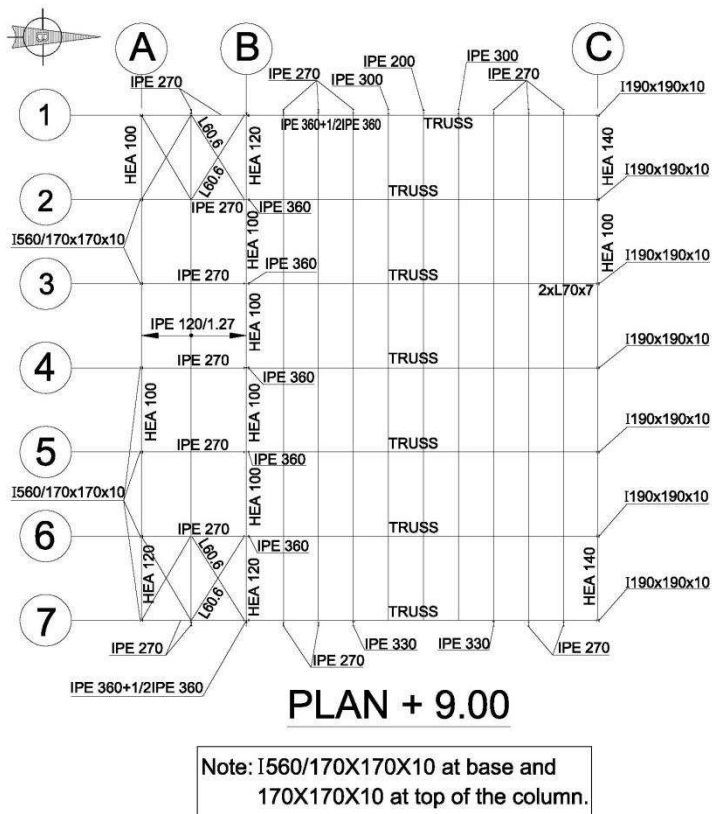
a)



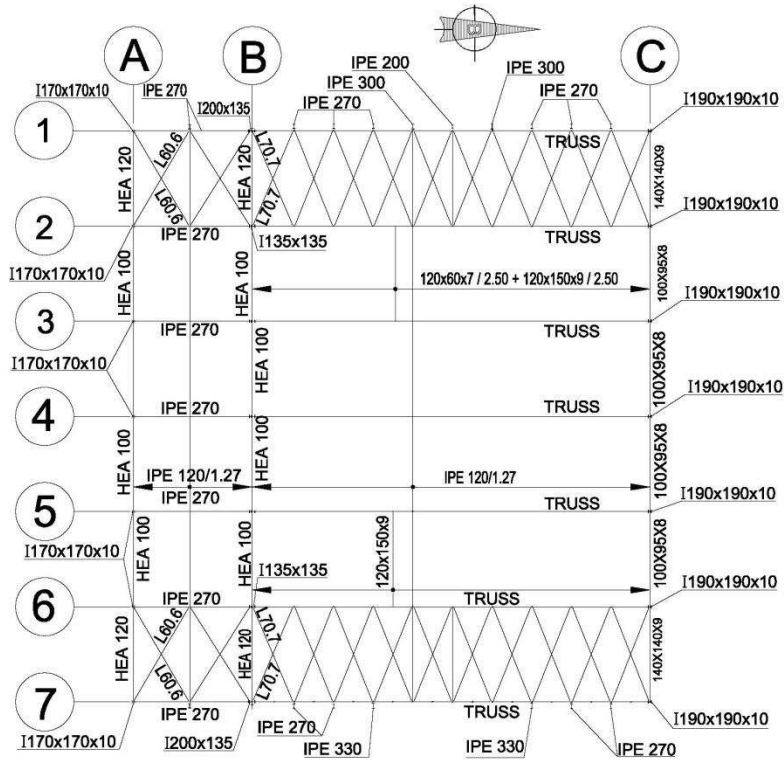
b)

Fig. 2. a) Overall view and b) structural details of the steel lattice roof.

(a)

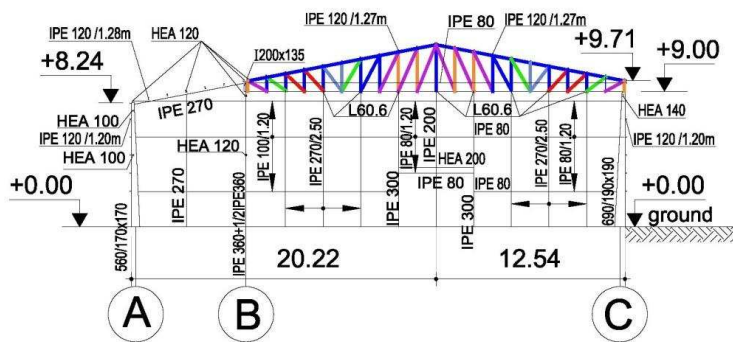


(b)



PLAN ROOF

(c)

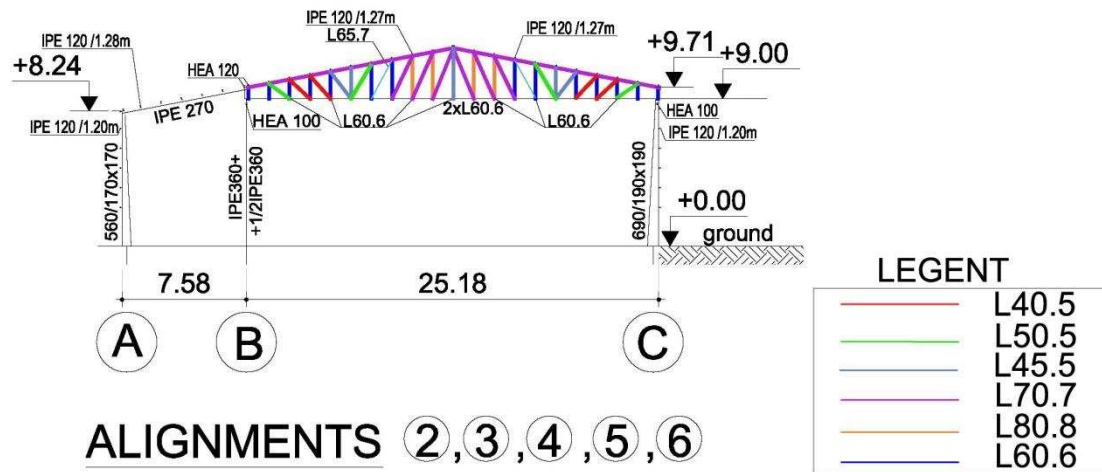


ALIGNMENTS 1,7

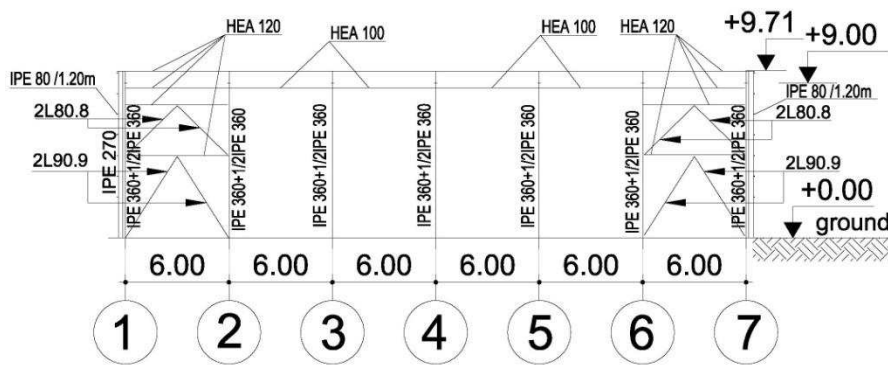
LEGENT

	L40.5
	L50.5
	L45.5
	L70.7
	L80.8
	L60.6

(d)



(e)



(f)

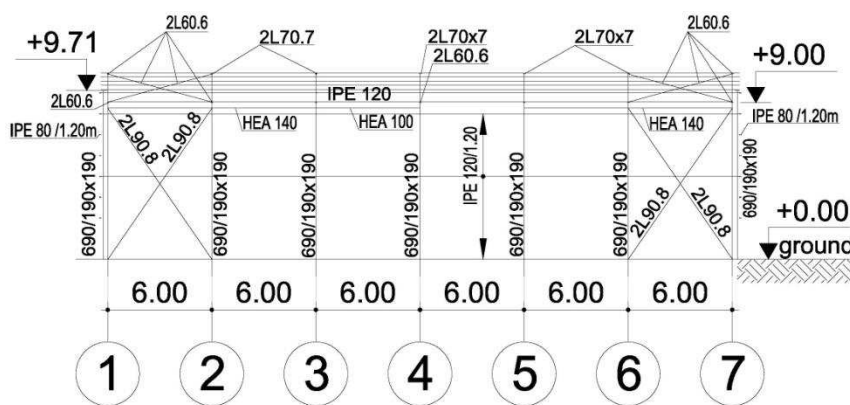


Fig. 3. Drawings of the studied steel structure (a) plan at level +9.00, (b) roof plan, (c) alignments 1 and 7, (d) alignments 2 to 6, (e) alignments A, and (f) alignment B and C

Vertical and horizontal bracings from the double angle sections are located at the end openings of the longest direction of the structure. Insignificant secondary H-type beams are located between the columns of the frames while the trusses are connected in the longitudinal direction through I-type purlins and L-sections at the top and bottom chords, respectively. Gable columns with sections ranging from IPE200 to IPE330 are used to support the large areas at the east and west sides of the building. S235 structural steel is used for all existing steel members.

Prior to the structural assessment of the gravitational load-bearing capacity of the building, a field-survey was performed in order to record existing structural damages (phase A of the Study), as described in detail in section 2.1.

2. Results and Discussion

2.1 Structural assessment of the existing structure

2.1.1 Survey and theoretical study

During the field-survey of the existing structure, a detailed record of the damages of the superstructure was created after examining the foundations. Significant damage was visually observed; an overall view of the structural condition is presented herein:

a) Extended buckling deformation of the corroded Λ -type vertical bracings to the south (Fig. 4a) as well as of the connecting beams between the IPE360 columns at +8.70 m (Fig. 5).



a) b)
Fig. 4. Vertical Λ -type bracing on the southern section of the building: a) the corroded portion with major second-order deformation and b) the undamaged portion.





Fig. 5. Steel elements with major second-order deformations.

- b) Column-baseplate connections with major corrosion effects and insufficient stiffener thicknesses (Fig. 6a).
- c) Significant cracking effects at various locations along the perimeter of the brick wall. In particular, shear cracking expands to the concrete foundation wall on the north-east corner (Fig. 6b).
- d) Relaxed bolted connections at elements of major importance (i.e., vertical bracings) as well as relaxed anti-sag bars at the roof (Fig. 7).
- e) Major torsional deformation of vertical primary elements with insignificant torsional stiffness (Fig. 8).
- f) Almost non-existing column foundation under the first and last truss. They were connected to a slim (~20cm) layer of plain concrete without any reinforcement.



a)



b)

Fig. 6. Bad condition of the existing structure a) Column base with significant corrosion and b) brick wall with a large crack.



Fig. 7. Relaxed bolted connection.



Fig. 8. Insufficient beam-column connection.

The peak velocity wind pressure (imposed load) according to the Eurocode (EN 1991-1-4) [14] was estimated as $q_p = 2.1 \text{ kN/m}^2$ for a height of +12.0 m. Based on this, the total force along the longitudinal direction (west-east) is approximately 700kN.

The commercial software Staad Pro [15] was used to perform the structural analysis and design of the existing structure. More details are given in the follow sub-section.

The results indicate the significance of this study as 610 out of 1324 beam elements do not satisfy the Eurocode requirements [14, 16-18]. Out of these, only 39 critical inadequacies occur due to seismic action, while the most unfavourable structural performance occurs as a result of the wind loading. The resistance ratios are significantly exceeded in the bracings and the main chords of the lattice roof.

This is expected, as the seismic action for 0,16 g peak ground acceleration, ground type A and $q=1.50$ is low due to low mass participation of the structure. On the other side, the wind force is higher than the seismic force and unfavourable for 33 m/s wind speed according to EN1991-1-4 [14], without any barrier due to structure geometry. Both loads are considered for the same return period and safety level according to Eurocodes.

In addition to the main structure, Building B contains an independent steel structure used for seating that was constructed more recently (after the main building). No failures were observed in this structure during either the survey or the desk study.

In summary, this investigation indicated that corrosion (Fig. 4) and construction (Fig. 7 to 9) defects as well as accumulated damage (Fig. 4) from past events and further deterioration combined to produce the present structural condition. It is likely that failures of different structural elements (i.e., brick walls, bracings, etc.) resulted from different events that took place in an unknown sequence. Nevertheless, it is vitally important to examine the most likely sequences that could lead to failure before proposing strengthening measures. Since the most severe main steel structure failures are caused by the wind, more detailed numerical simulations are conducted in section 2.3.

2.2 Materials and methods

A small variety of the materials was found. As it was aforementioned, S235 structural steel was used whereas the concrete foundation and bottom slab meets the concrete properties (C25/30) as required by the code. The materials used in the existing structure were used through the numerical calculations.

For the needs of the current study, several numerical procedures were implemented, each one depending on the purpose of the investigation. Thus, five different simulations were conducted, namely: i) linear static analysis, ii) linear dynamic (modal) analysis, iii) non-linear dynamic (time-history) analysis, iv) non-linear incremental static (pushover) analysis, and v) non-linear buckling analysis. For the above simulations three different commercial software

were employed (Staad Pro [15] for cases i-ii, Sofistik [19] for cases iii-iv, and Abaqus [20] for case v).

The first two (linear) methods are conducted via Staad Pro, for the needs of the design according to Eurocodes. The structure was simulated as a 3D model with beam elements for beams/columns and truss elements for bracings and trusses, while moment releases were introduced where necessary. The materials have linear (elastic) properties ($E = 210$ GPa). The wind and snow loads are transferred to the main structure through purlins and side rails. The wind loads considered for zones (A, B, C, D, E +roof), wind speed 33 m/s, terrain seaside, height +0 m, wind direction longitudinal/lateral with main direction are shown in Fig. 10.

To perform the transient time-history analysis, random wind histories were generated based on the Karman wind spectrum [21] using the “sofiload” module of the commercial software Sofistik [19]. The spatial coherence of fluctuating wind fields were taken into account. The non-linear material properties of S235 structural steel were simulated for critical members such as the vertical bracings along the Y-direction (Fig. 10). In particular, the stiffness and resistance in compression or tension are estimated separately for each member, whereas the stiffness in shear and bending are negligible compared to the axial ones.

An incremental non-linear static analysis (pushover) was performed in order to understand the total bearing capacity of the structure. The material properties defined for the time-history analysis were applied alongside the displacement shape vector from the first step of the time-history analysis instead of using a fundamental eigenmode of the structure. The target lateral forces were defined according to wind load pattern from EN 1991-1-4 (Karman spectra parameters were $a_1=4$, $a_2=0$, $c=2$, $X=fL/v$ for both directions and at the longitudinal direction $a_3=0$, $b=70.8$, $d=5/6$ and at the lateral direction $a_3=3021$, $b=283$, $d=11/6$, 10 different spectras used).

The Karman [21] spectra is defined by the equations:

$$\frac{f \cdot S}{\sigma^2} = \frac{a_1 \cdot X + a_2 \cdot X^2 + a_3 \cdot X^3}{(1 + b \cdot X^c)^d} \quad (1)$$

$$X = \frac{f}{f_m} = \frac{f \cdot L}{V} \quad (2)$$

Where L is the effective wavelength defined with the wind profile and f_m is the effective frequency of the turbulence. Spectra from Kaimal use for X the Monin coordinates, replacing L by the height z. The shape of the spectra is changing for different directions, therefore the

six coefficients $a_1, a_2, a_3, b_1, b_2, c$ are defined for three components. The Karman's distribution [21] is presented in Fig. 9.

The coherence was taken by the equation:

$$\sqrt{\text{coherence}} = \gamma_{uu}(\Delta x) = \exp\left(-a_{ii} \frac{f \cdot \Delta x}{V}\right) \quad (3)$$

Where uu is the studied wind direction y .

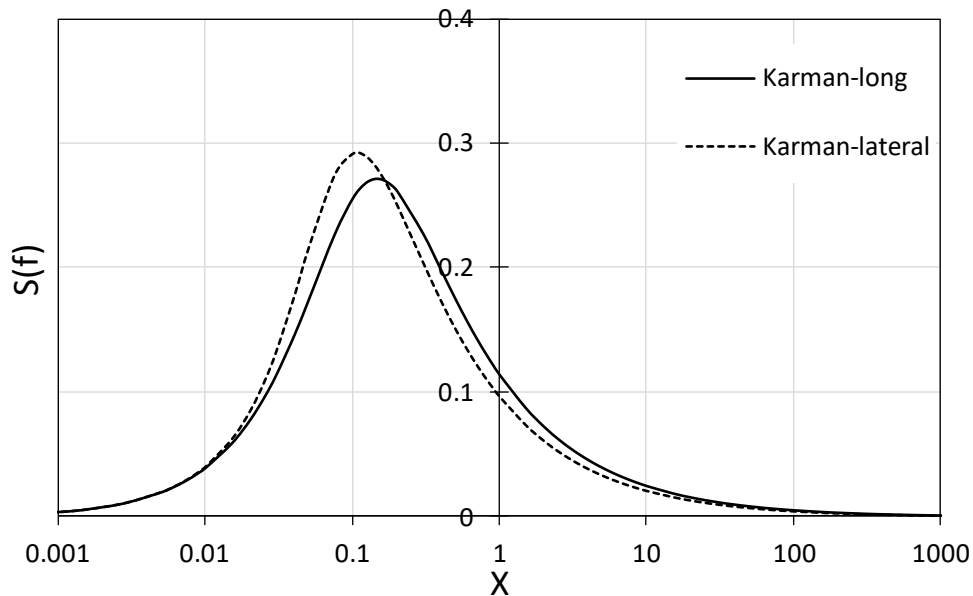


Fig. 9. Karman's distribution of S as a function of X [21]

Obtaining the response of the damaged vertical bracing to the 10 min wind time-history analysis, the buckling capacity was estimated in a more precise manner via a detailed finite element (FE) simulation, according to modelling techniques presented in the literature [22]. For this reason, a double L79x79x7 cross-section was simulated in Abaqus [20] using the material model ($f_y/f_u = 235/360$ MPa and 0.20 ultimate strain) which is also connected back-to-back through packing plates, as was noted on-site. The effects of the non-linear geometry were also taken into account during the displacement-based incremental analysis (via the Static General module). The steel member considered with $L/250$ global imperfections as defined by EN1993-1-1 [17] in both directions.

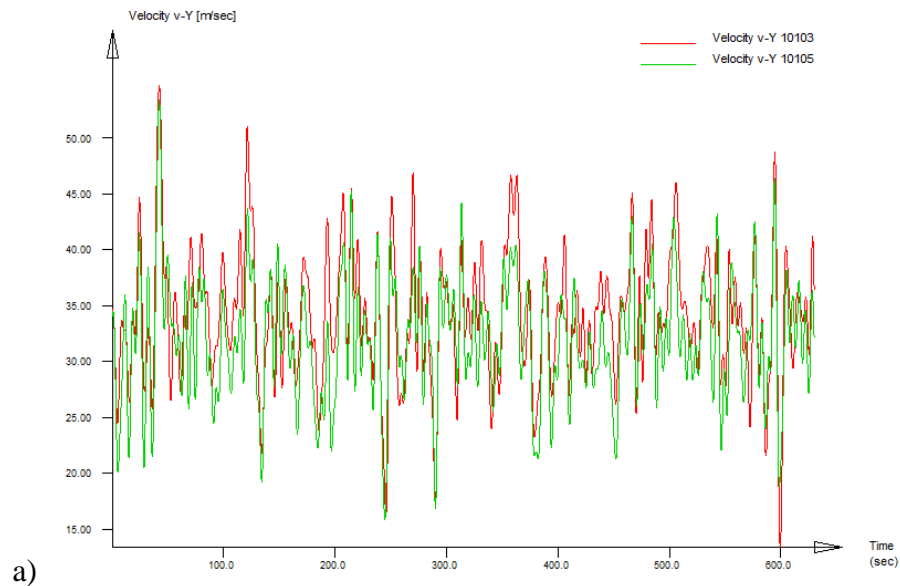
2.3 Specialised numerical simulations

Wind loads are characterised by randomness in both time and space. A close examination allows one to observe that wind records consist of a mean-value plus random wind speed fluctuations. Furthermore, a short wind gust may trigger a considerable dynamic

response, for which a deterministic view of the design code cannot provide an accurate prediction. In the current work, the existing second-order deformations from the case-study are thoroughly investigated via the wind time-history and non-linear buckling analyses presented in the next sub-sections.

2.3.1 Wind time-history analysis

The wind profile corresponds to that of a coastal area with a mean wind velocity of approximately 33 m/s operating for 10 min (similar to the wind profile defined by EN 1991-1-4) [14]. The time-histories for structural elements at heights of 5 m along the long and transverse directions of the structure are depicted in Fig. 10. Ten different wind spectra used in order to avoid non-conservative analysis.



a)

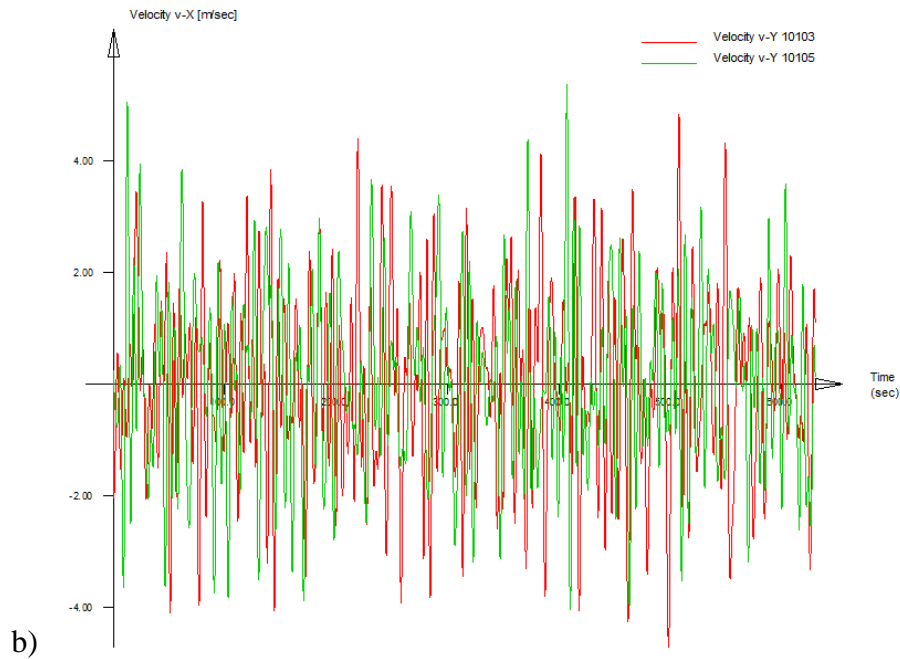


Fig. 10. Typical velocity time-history samples for the a) longitudinal and b) transversal wind directions.

The wind load in the longitudinal direction is simulated only for the Y-axis since major building damage has been observed in this direction in particular. The vertical component of the wind load is not considered in the present study. In Fig. 11, the 3D view of the existing simulated structure is shown as well as the element numbering for 4 selected bracings.

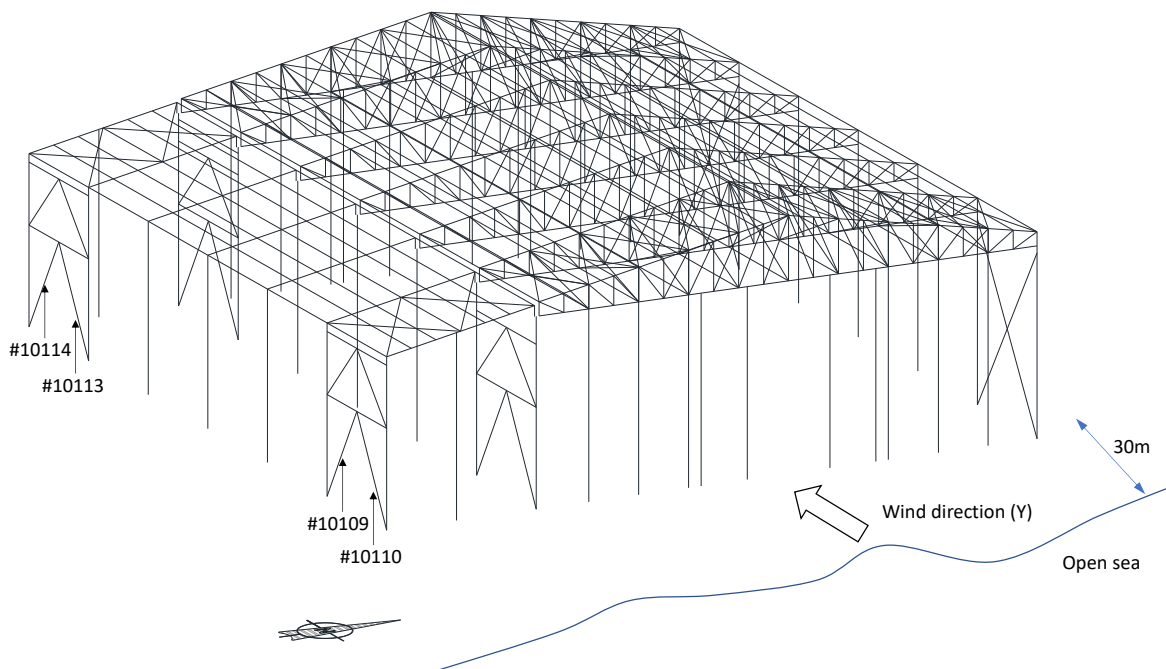
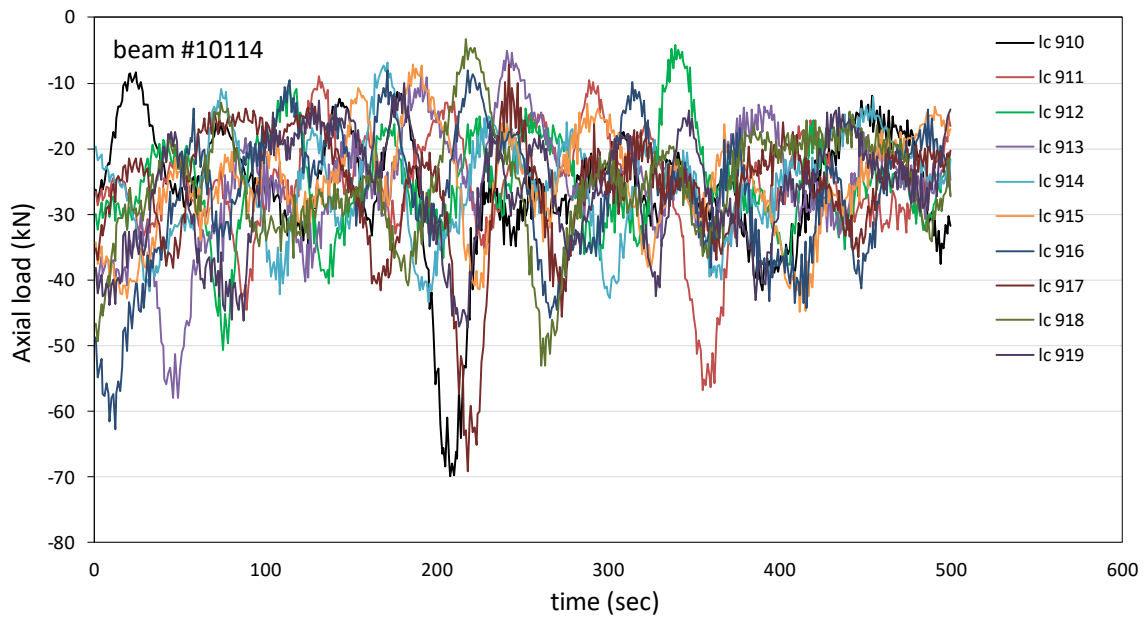


Fig. 11. The overall configuration of the existing structure.

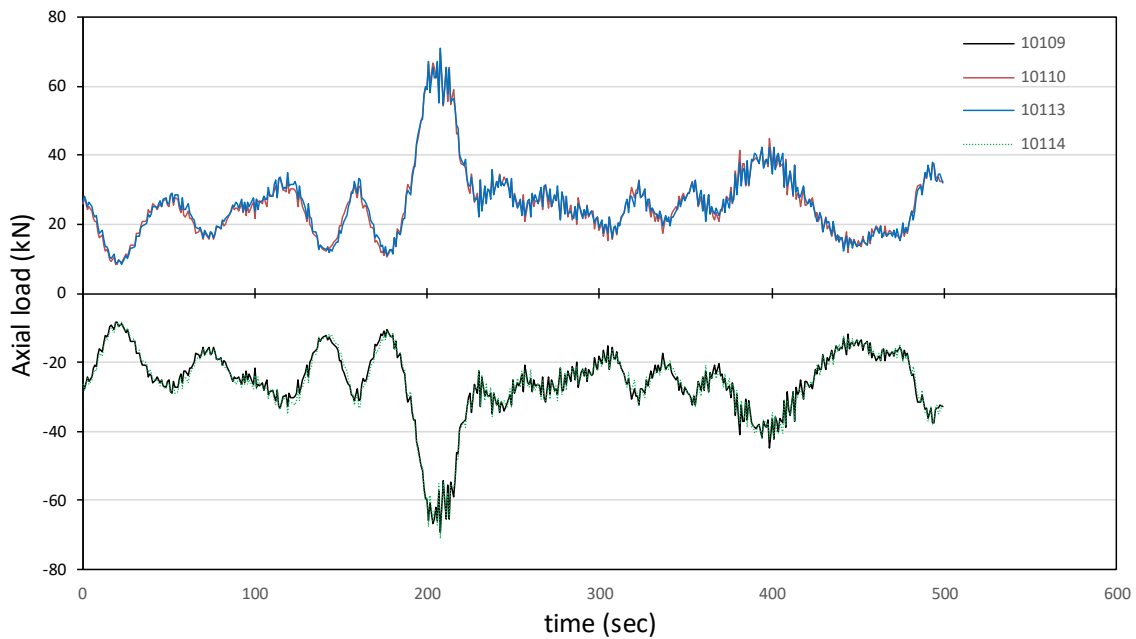
An interesting clue appears to significantly affect the structural response with regard to excessive second-order deformation of the south-west lower bracing [member no. 10114 presented in Fig. 4(a)]. The stiffness and vertical load capacity of the damaged member are obtained from FE buckling analyses using Abaqus [20]. The results are presented in section 2.3.2.

The results of the time-history dynamic analyses for the selected beam elements in terms of axial force are presented in Figs. 12(b) and 12(c). Figure 12(a) shows the axial forces developed on element 10114 (failed element) during the time history analyses performed for the 10 different wind spectras. The two figures (12(b) and 12(c)) respectively address conditions that exclude and include geometrical imperfection from the buckled L-section. The latter case can be referred to as the "imperfect" one. A thickness reduction of 1.0 mm due to corrosion is also included in this case. One can clearly observe relief of the damaged and tensile (member no. 10113) members. In contrast, the east pair of bracings displays additional axial force, which reveals a more unfavourable design status (member nos. 10109, 10110). The axial forces are differentiated by approximately $\pm 45\%$.

(a)



(b)



(c)

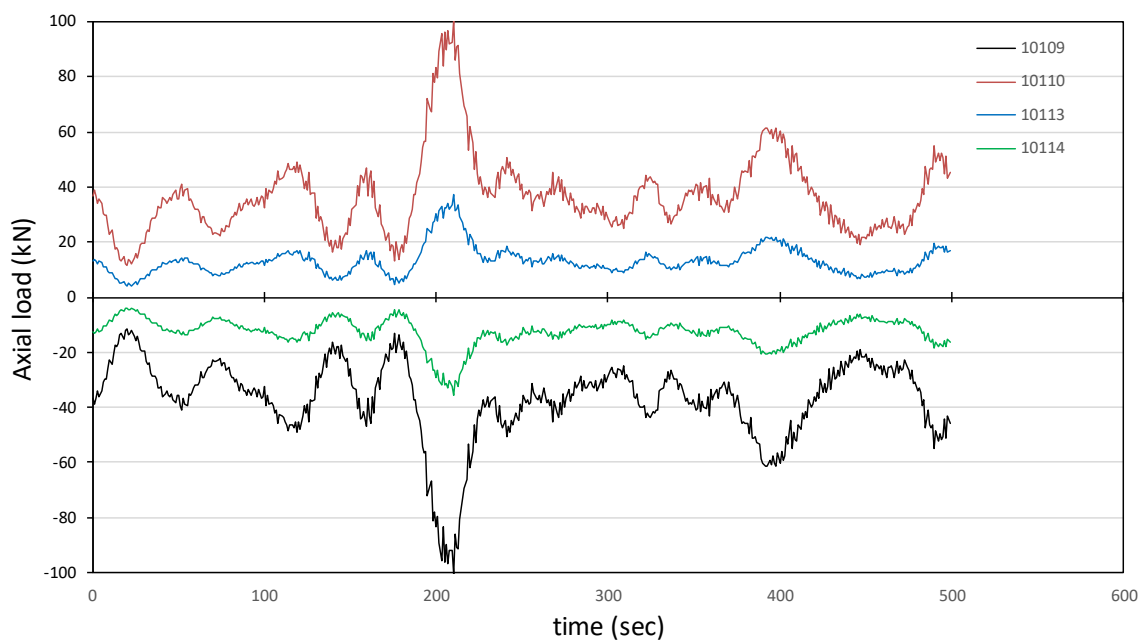


Fig. 12. Axial load histories for Λ -type vertical bracings with a) axial force developed on element 10114 for 10 different wind spectras and b) perfect structure axial loads of bracing elements 10109, 10110, 10113 and 10114 for the most unfavourable time history and c) imperfect structure axial loads of bracing elements 10109, 10110, 10113 and 10114 for the most unfavourable time history.

The axial force and dynamic histories as well as the axial displacement history determined via the dynamic analysis, are shown in Fig. 13. The maximum recorded load is 71.0 kN, which corresponds to axial shortening of 31.6 mm. The shortening itself ranges

from 4.0 to 36.7 mm. Considering only the axial load produces a surprising outcome since the maximum developed compressive force does not exceed the buckling capacity of the corroded bracing. However, a design engineer should cautiously consider the most critical qualities, which are the motives for a displacement-based analysis.

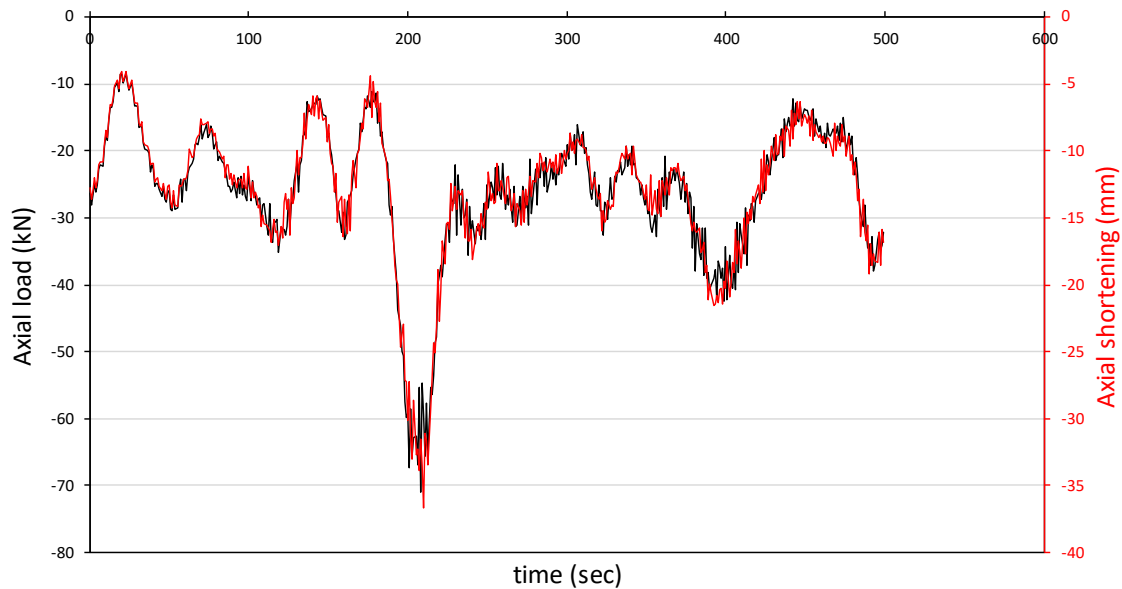


Fig. 13. Axial load and displacement response of element no. 10114.

2.3.2 Vertical bracing buckling capacity

The buckling response, as shown in Fig. 14, was identified after importing the exact function of the axial displacement from the wind history analysis into Abaqus as a boundary condition amplitude. The maximum buckling capacity attained is greater than 81 kN (greater than 71 kN from Fig. 13). Nevertheless, buckling phenomena have occurred due to a significant shortening of the beam. In addition, the axial stiffness of the buckled beam is confirmed using the post-buckling curves. In particular, the stiffness (which is detected at the onset of a new compression region) is nearly equal for all subsequent loading paths after the first buckling occurrence (axial displacement of 3 mm).

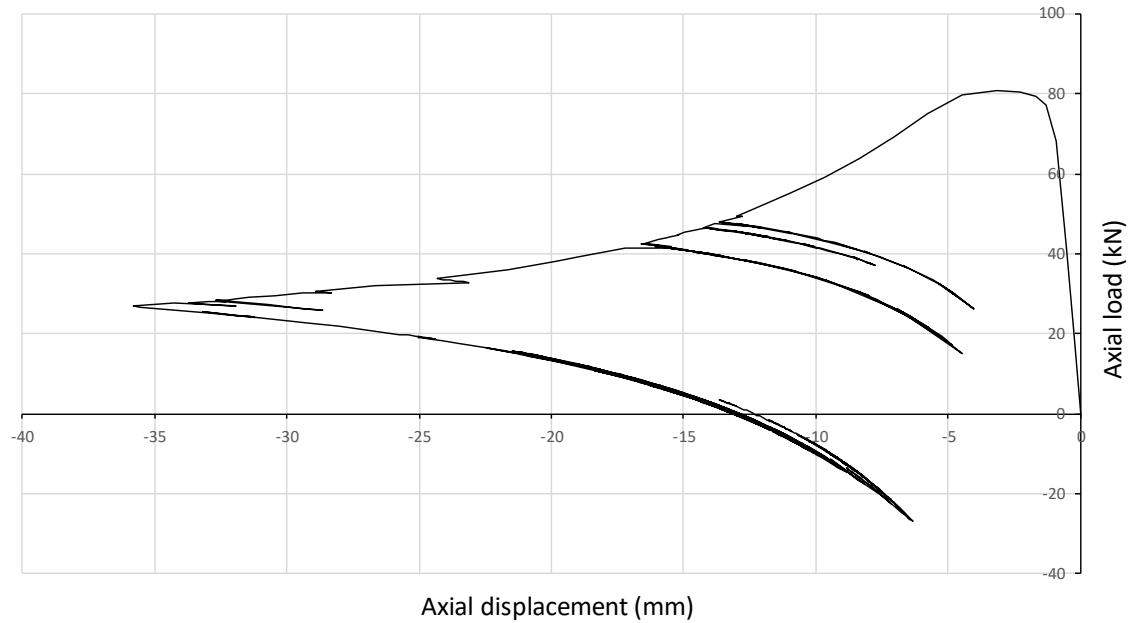
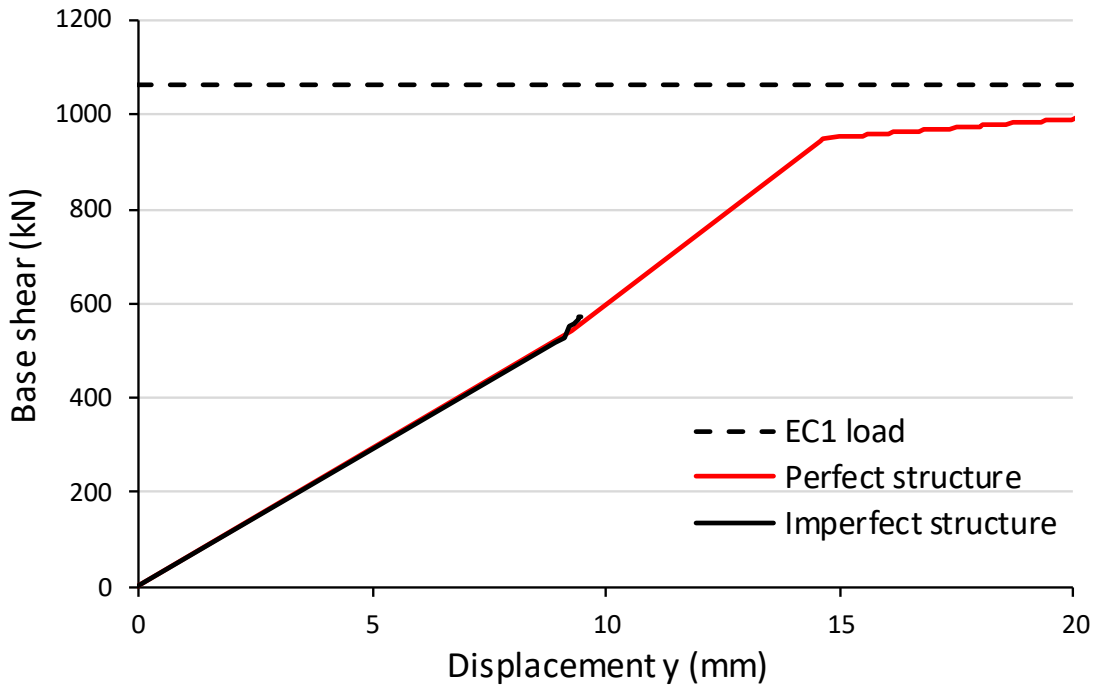


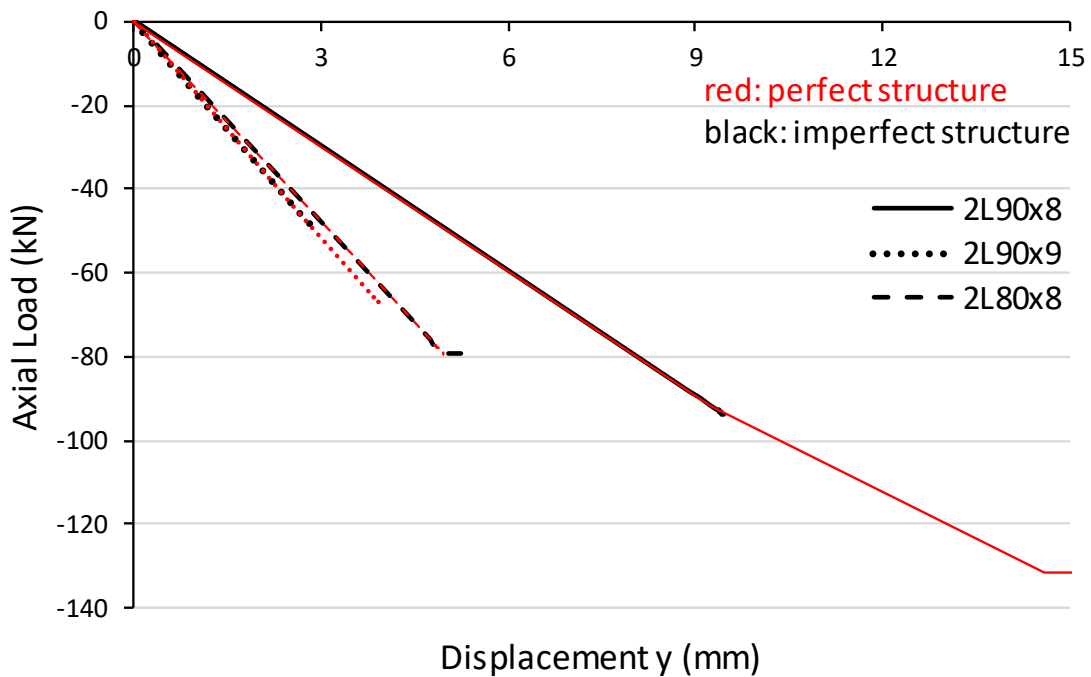
Fig. 14. The response of the corroded buckled bracing, as determined using Abaqus.

2.3.3 Vertical load capacity curves of the existing structure

The vertical load capacity curves are shown in Fig. 15(a) capture the total response of the structure, while the dashed line defines the minimum requirement that the structure should have met. After considering imperfections, i.e., excessive deformation of the damaged bracing, the bearing capacity is only 58% of the perfect sample. Nevertheless, the latter vertical load capacity does not satisfy the Eurocode requirement in terms of the total base shear force. Furthermore, the axial load-displacement curves of the major vertical bracings are compared in Fig. 15(b), while the selected imperfection is neglected during pushover analysis. The double equal angle cross-sections L90x8, L80x8, and L90x9 correspond to the existing bracings of the north, south, and Section 1-1 views, respectively.



a)



b)

Fig. 15. Comparison of the a) vertical load capacity curves and b) axial load-displacement paths of vertical bracings within perfect and imperfect structures.

3. Retrofit proposal

Critical structural interventions proposed as a result of the study are outlined below. Points a through c refer to angle cross-sections members.

a) Addition of horizontal X-bracings near the roof ridge (roof plan view in Fig. 16, Fig. 17).

- b) Addition of vertical bracings between the roof trusses for reasons of lateral restraint, as well as between the south 560/170x170 and IPE360 columns (for east and west side-views) for serviceability limit reasons.
- c) Replacement of insufficient vertical bracings using the same or different configurations (examples from the south and north sides of the building as well as Section 1-1 can be observed in Fig. 16, Fig. 17).
- d) Replacement of distorted members such as H-type connecting beams in Section 1-1 of Fig. 16, Fig. 17.
- e) Replacement of vertical elements at the end of the IPE360 column (Fig. 17), which is predicted to provide a stiffer beam-column connection.
- f) Strengthening the cross-sections of the main chords of the lattice roof using thin-walled hollow sections. Strengthening of specific truss members by adding second angle sections [Sections 2-2 and 3-3 in Fig. 17 and details in Fig. 18(b)].
- g) Replacement of purlins and a denser arrangement or replacement of side rails.

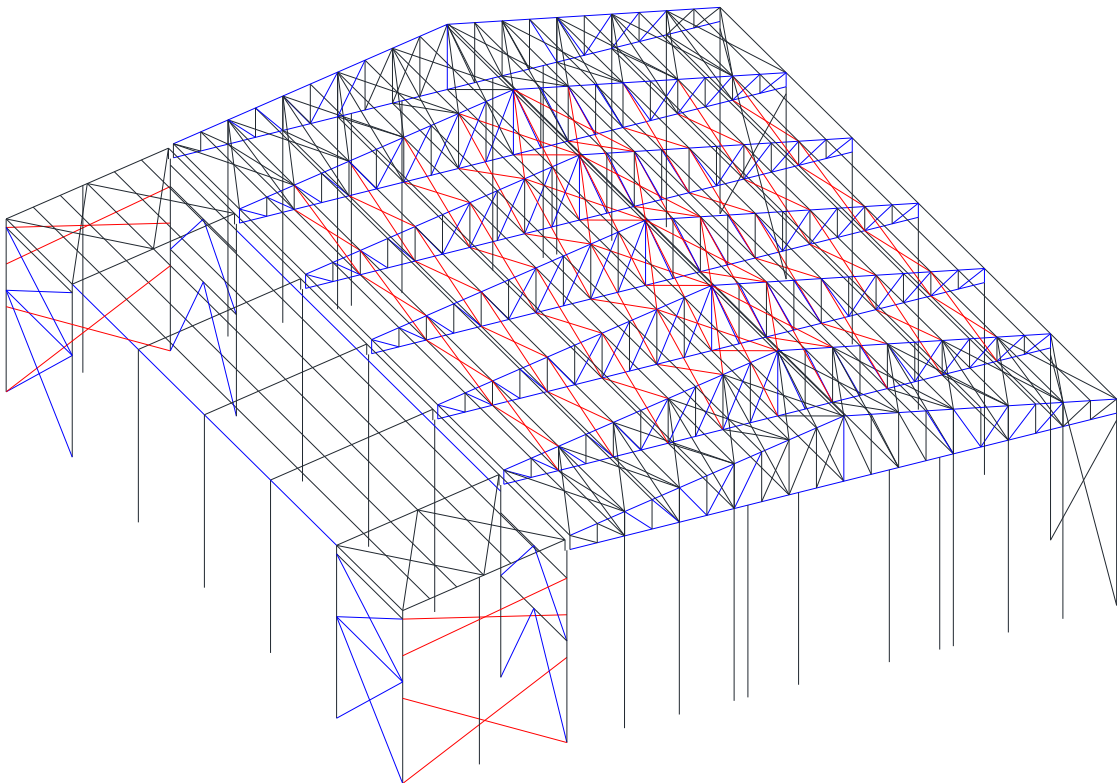


Fig. 16. Three-dimensional view of the structural modifications (blue for replacement or strengthening, red for member addition).

Fig. 16 shows the type and extent of interventions recommended for the main steel structure. Replacement and strengthening of the truss roof are illustrated in blue, while red is

used to indicate member additions. The same conventional symbolism has been adopted for Fig. 17. Some serviceability constraints (e.g., equipment, etc.) prevent the use of a more orthodox and appropriate X-bracing configuration in the east and west views (outer red vertical bracings in Fig. 16).

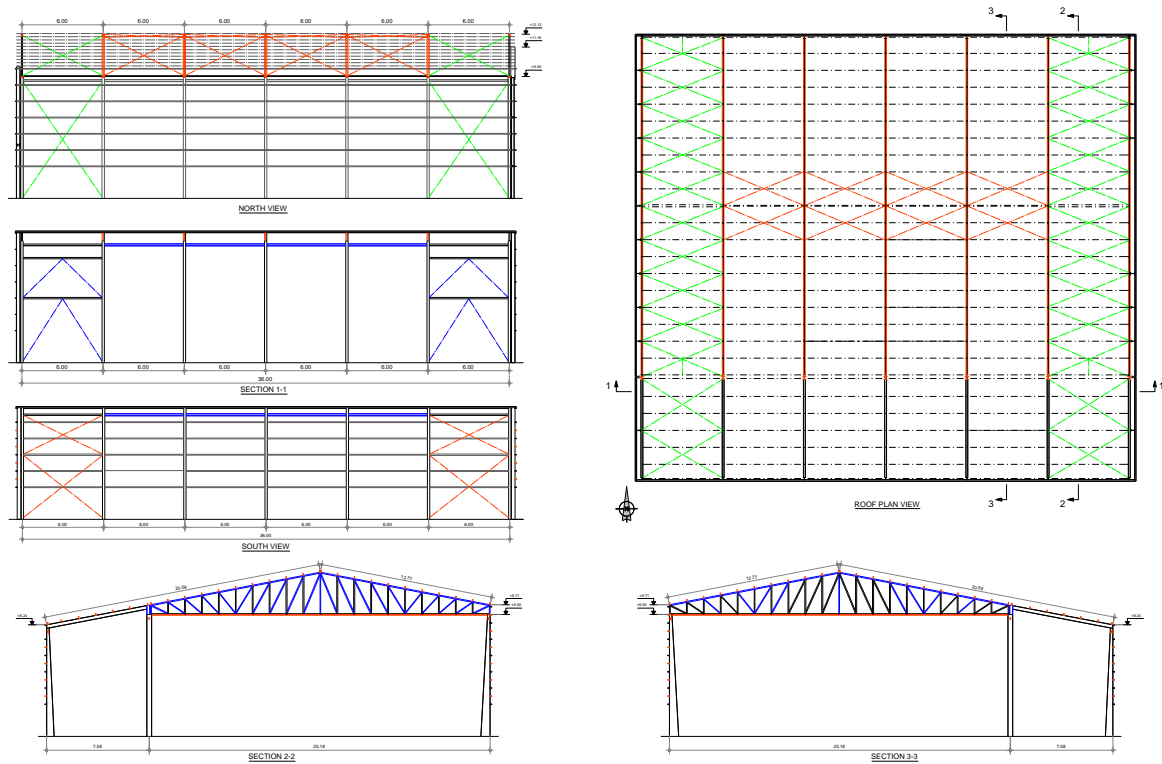


Fig. 17. Schematic view of the strengthened structure (green for existing bracings, red for proposed modifications, and blue for strengthening).

Minor but important restoration techniques should be implemented. They include tightening of bolts and anti-sag bars, surface treatment for corroded members that are not to be replaced (e.g., surfaces of columns near the base). Special treatment for foundation inadequacies is required as well. In particular, portions of the foundation beneath the gable columns (at both the east and west parts of the building) should be strengthened so that they can receive bending moments. The latter recommendation is illustrated in Fig. 18(a), where H-type steel beams are used as provisional column supports for an adequate length in both directions.

A detailed schedule of strengthening of the truss chords (point “F” of the strengthening proposals) is attached in Fig. 18(b). The new hollow sections will be properly welded under the existing angle members since the purlins and the web members used for the upper and lower chords of the truss, respectively, preclude any other recommendation. Finally, it is

pivotal to maintain a light-weight design with scope to optimise the bearing capacity of the lattice structure.

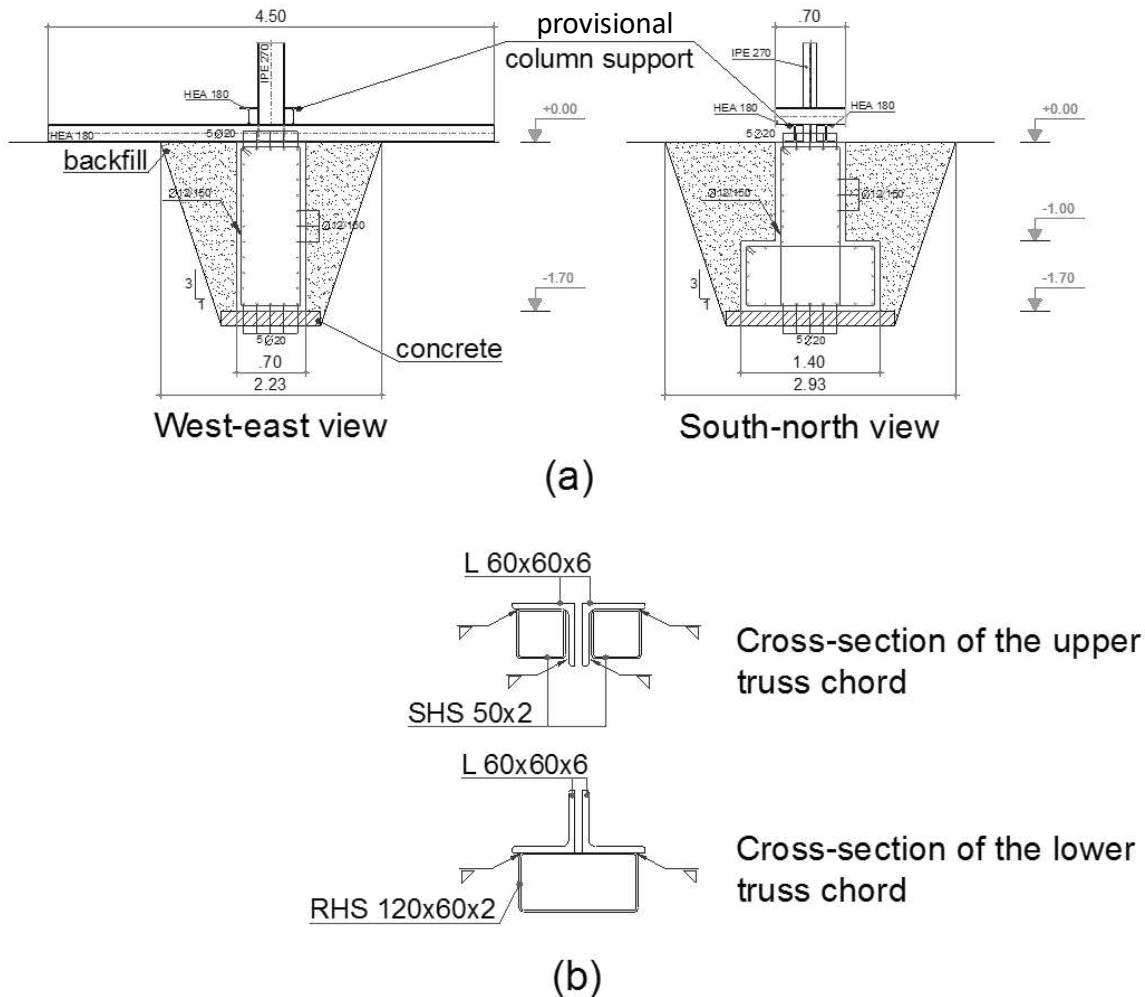


Fig. 18. Schematic view of strengthening details for a) the foundation and b) the truss chords.

4. Structural performance of the strengthened structure

Analytical results for the structural response of the strengthened structure suggest that all design requirements are satisfied for cases of ultimate (ULS) and serviceability (SLS) states. In particular, the maximum vertical displacement of the roof is limited to 37 mm (compared to 69 mm in the existing structure) for serviceability limit state combinations caused by wind. With regard to horizontal displacements, the maximum drift of the structure under seismic excitation is limited to 30 mm, rather than the 75 mm experienced before strengthening.

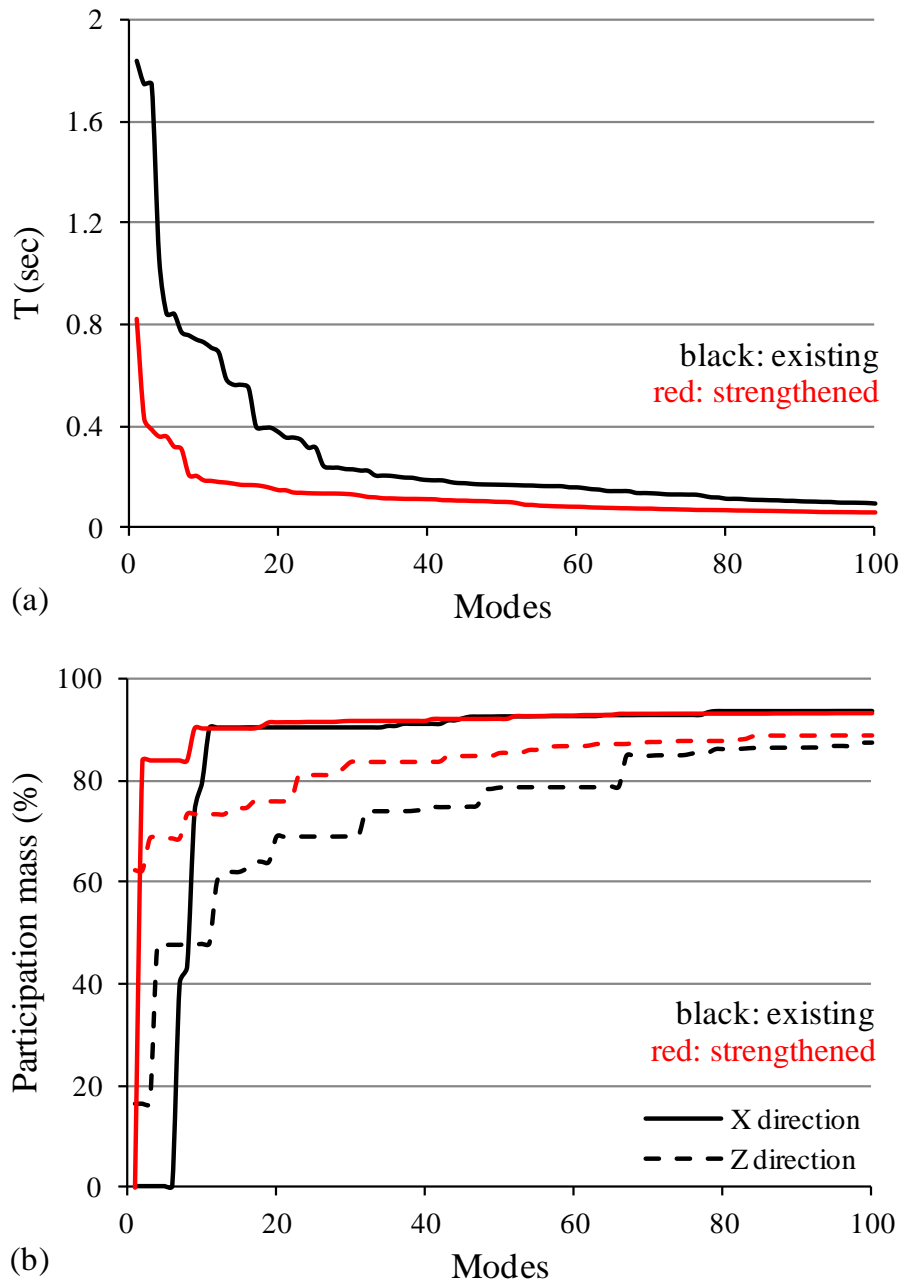


Fig. 19. Comparison of the dynamic characteristics of the existing (black) and strengthened (red) structure (solid and dashed lines for the X- and Z-directions respectively).

Modal analyses [23] have been performed to compare the existing and strengthened structures. The results are shown in Fig. 19 demonstrate clear improvement to the dynamic characteristics of the structure. In particular, mass participation is increased to 62% and 84% in the long and transverse directions (along Z- and X-axis, respectively), compared to 31% in the unstiffened structure. The corresponding periods decrease from 1.07 s to 0.82 s and from 0.74 s to 0.43 s along Z- and X- directions, respectively, after the proposed retrofit. The aforementioned mode shapes for the long and transverse directions are compared in Figs.

19(a),(b) and Figs. 19(c),(d), respectively. In addition, Figs. 19(a),(c) and Figs. 19(b),(d) demonstrate the existing and strengthened structure respectively.

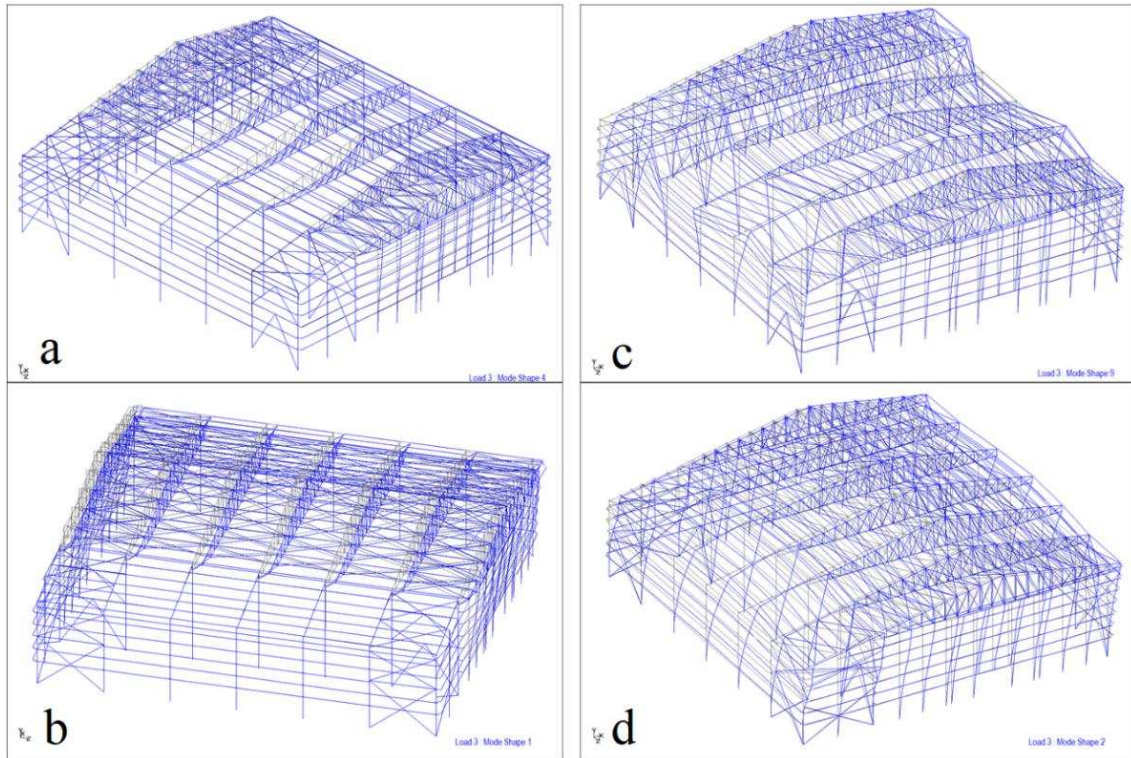


Fig. 20. Schematic view of some characteristic mode shapes of the existing (upper) and strengthened (lower) structures.

For the sake of completeness, the vertical load capacity curve of the proposed modified structure was established and compared to that of the existing structure. The procedure presented in Section 2.3.1, is repeated in Sofistik using the enhanced properties of the new and strengthened members. Fig. 21 depicts the new curve that indicates a total base shear force enlargement from 571 kN to 1571 kN.

Furthermore, Fig. 22 shows the axial force histories of bracing elements for the 10 different wind histories. In order to ensure that the analysis parameters are providing safe results, a sensitivity analysis for the coherence factor was performed and showed that the used coherence factor was appropriate (Fig. 23).

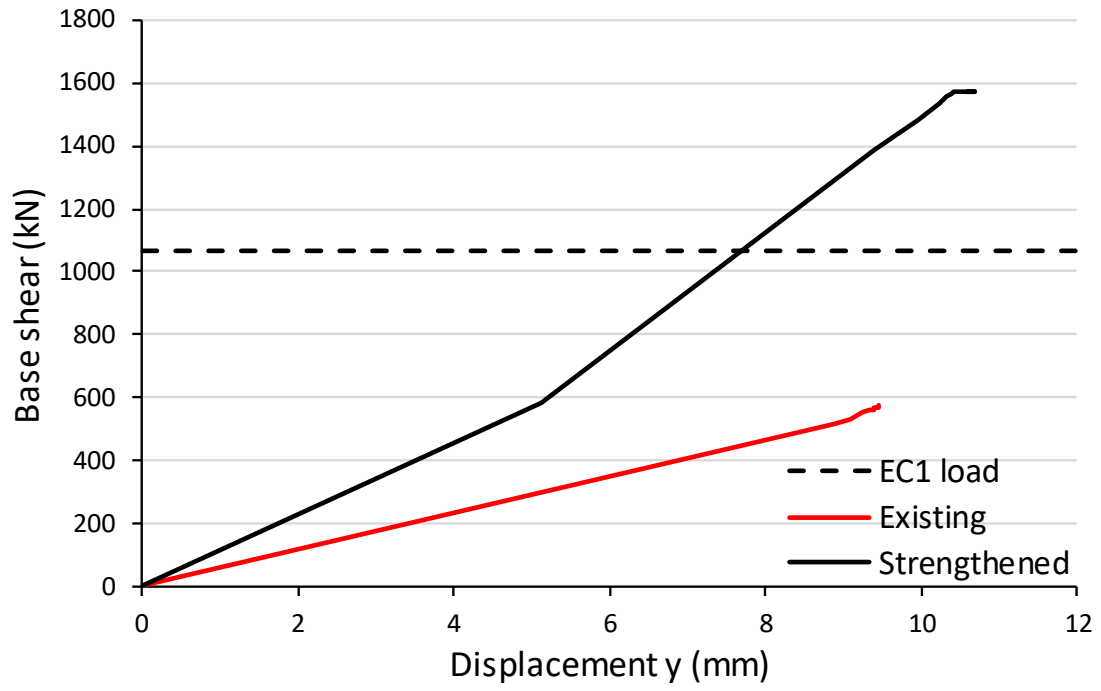
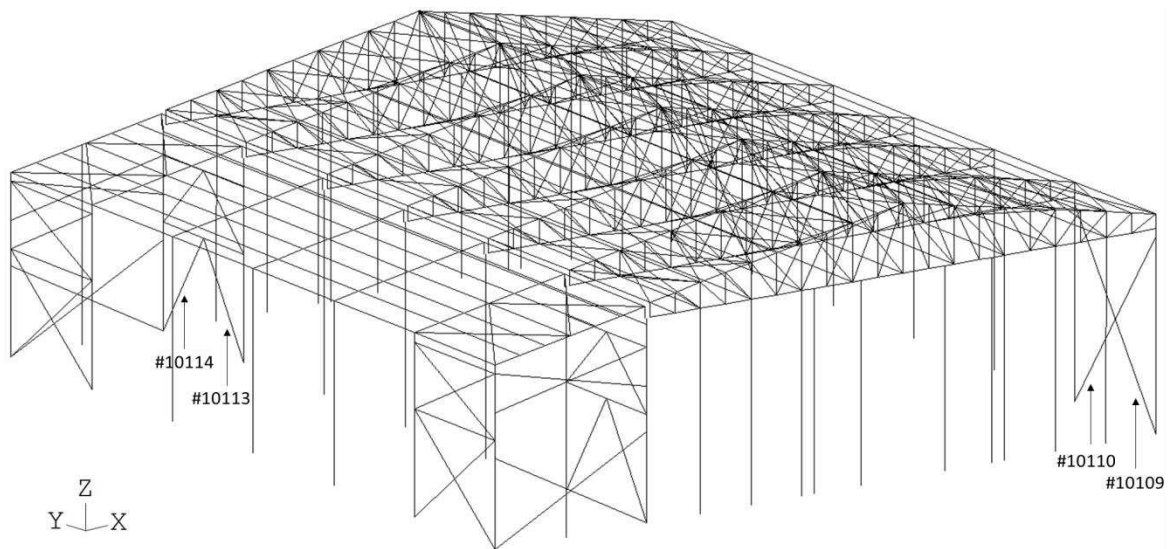
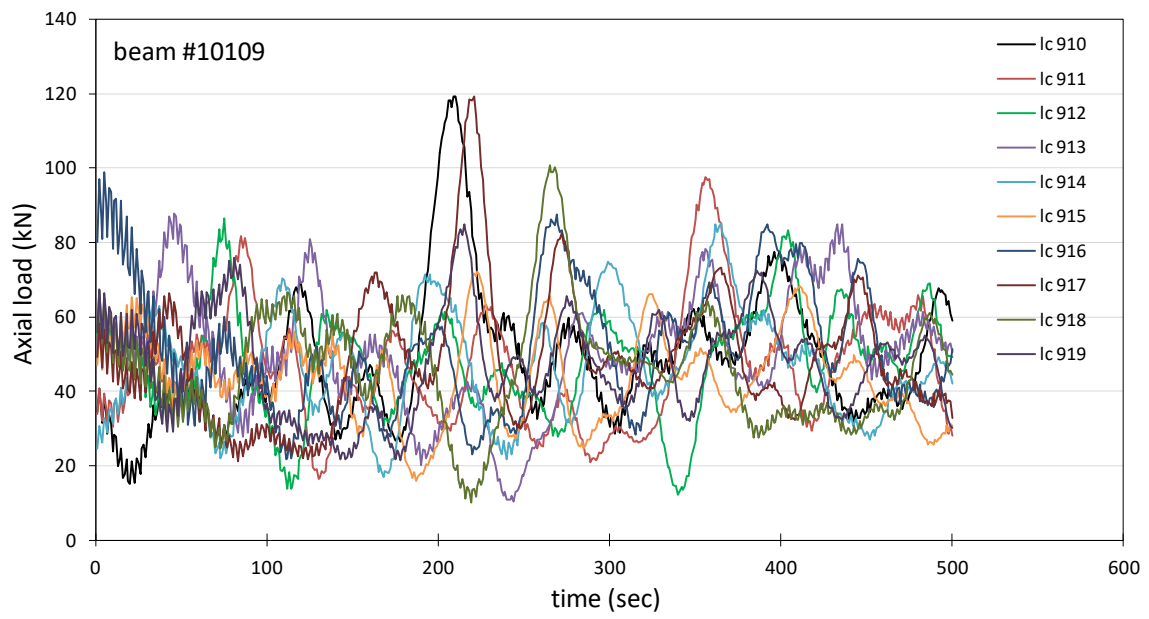


Fig. 21. Comparison of the vertical load capacity curves of the existing and strengthened structures.

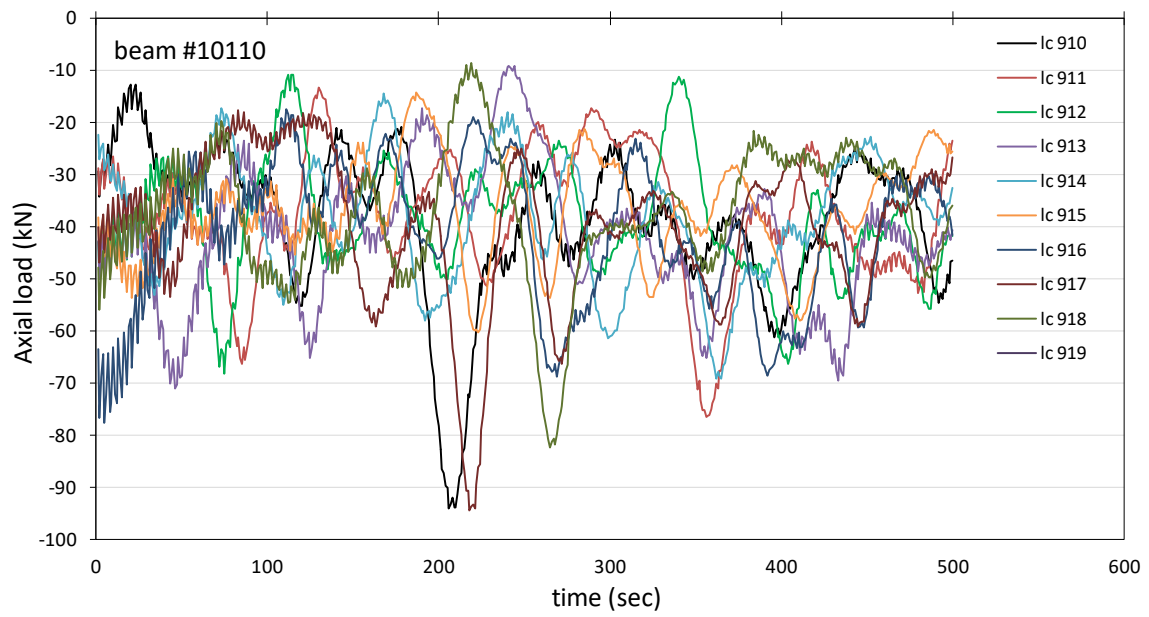
(a)



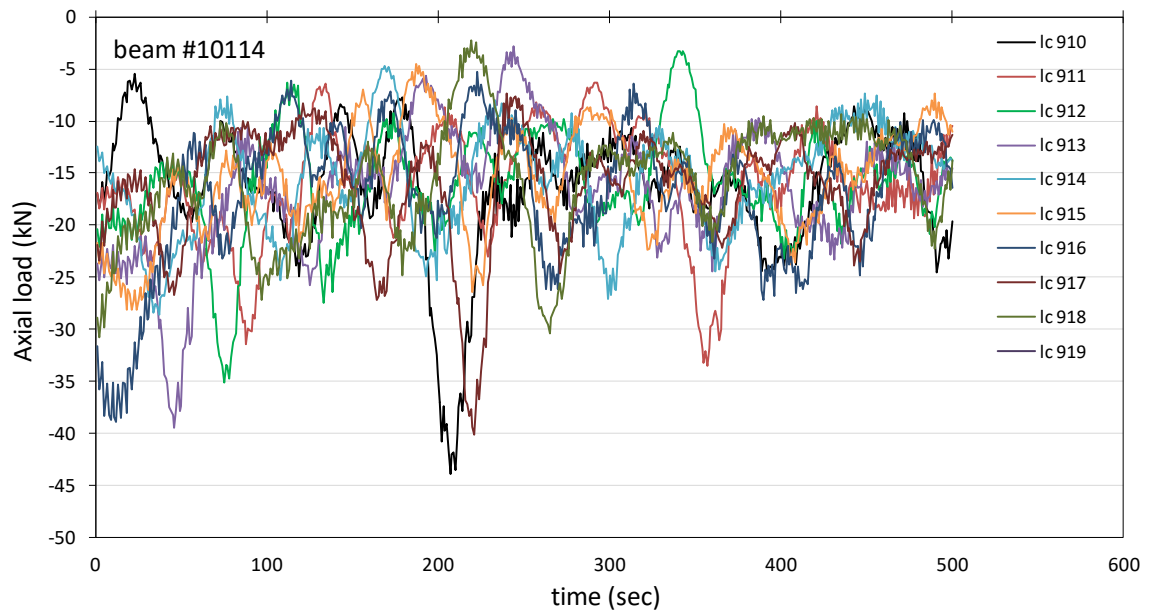
(b)



(c)



(d)



(e)

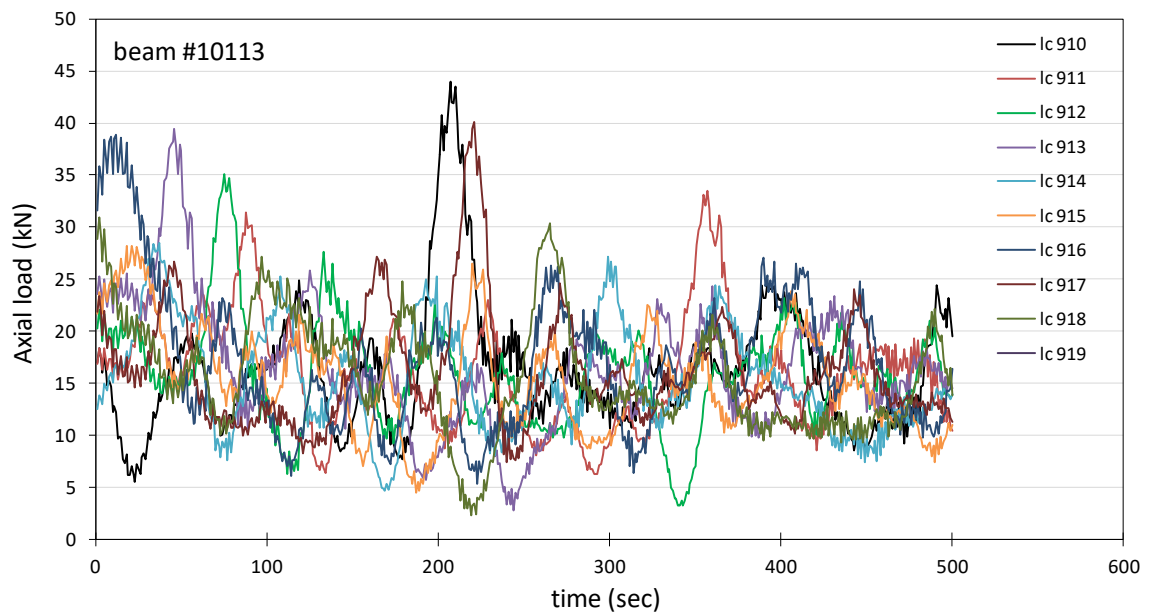


Fig. 22. (a) Strengthened structure numerical model with a number of bracing elements analysed, (b) axial force history of element 10109 for 10 wind time history analyses, (c) same for element 10110 (d) same for element 10114 and (e) for element 10113.

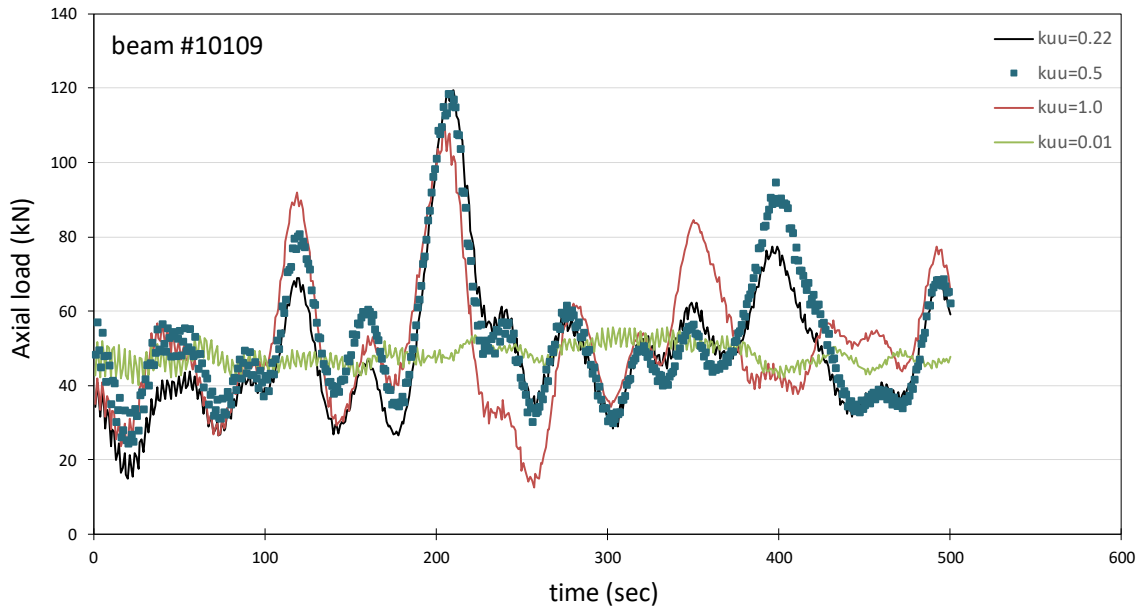


Fig. 23. Axial force history of element 10109 for different coherence factors.

4.1 Cost estimation of the strengthening proposal

It is worth noting that 14.9 tn of S275 structural steel was required for the strengthening of the main structure, while 22.8 tn of the same material was required for purlins and side-rails. The indicative cost for the structural steel (excluding purlins and side-rails) was around 41,000€ (31.5€/m² of the plan view) while the total repair cost included fees, taxes and unpredictable quantities approached 290,000€ (223.0€/m² of the plan view). Consequently, the difference between these values indicates that the major structural interventions are a relatively small part of the overall rehabilitation.

5. Concluding remarks

This study includes a structural assessment and strengthening proposal for an existing steel structure with major damages. During the rehabilitation project, detailed records and simulations were conducted in order to explain the structural deficiencies (such as excessive deformation, cracking, overstressing, etc.) that hinder the safety of the building. The results revealed crucial inadequacies as well as the need to strengthen (with a more accurate way) both the steel superstructure and the concrete foundation. Development of existing damage can be attributed to environmental factors such as corrosion and wind. No sufficient understanding of the sequence of failure events is available since changes made many years ago were not accompanied by further information.

Thus, advanced non-linear analyses were carried out in order to achieve more accurate structural behaviour. Non-linear time-history analyses conducted using artificial wind histories and non-linear incremental static analyses considering second-order effects illuminated the route from pathology and assessment to final treatment. A strengthening proposal was developed, along with other strengthening techniques for code-deficient steel structures [24], to make the rehabilitated structure comply with Eurocode regulations. A comparison of the existing and improved structure that highlights the dynamic response enhancement is presented. The increased bearing capacity is clearly illustrated via vertical load capacity curves obtained from the non-linear static (pushover) analyses, which highlights the margins of safety that can be expected throughout the remaining life of the strengthened structure.

An important lesson learned from this case study is that local weaknesses, construction mistakes, and corrosion may lead to unexpected failures when these are affecting critical structural elements. The unexpected loss of stiffness may also lead to torsional effects, redistribution of internal forces, and thereafter to failures.

6. References

- [1] SAMCO, Guideline for the assessment of existing structures, Final Report, 2006.
- [2] L.M. St. Pierre, G.A. Kopp, D. Surry, T.C.E. Ho, The UWO contribution to the NIST aerodynamic database for wind loads on low buildings: Part 2. Comparison of data with wind load provisions, *J. Wind Eng. Ind. Aerodynamics* 93 (1) (2005) 31-59.
- [3] G.A. Kopp, M.J. Morrison, B. Kordi, C. Miller, A method to assess peak storm wind speeds using detailed damage surveys, *Eng. Struct.* 33 (2011) 90-98.
- [4] F. Sadek, E. Simiu, Peak non-Gaussian wind effects for database-assisted low-rise building design, *J. Eng. Mech.* 128 (5) (2002) 530-539.
- [5] D.K. Kumar, T. Stathopoulos, Wind loads on low building roofs: a stochastic perspective, *J. Struct. Eng.* 126 (8) (2000) 994-956.
- [6] J.V. Retief, C. Barnardo-Viljoen, M. Holický, Probabilistic models for design of structures against wind loads, *Proceedings of the 5th SEMC Int. Conf.*, Cape Town, South Africa (2013) DOI: 10.1201/b15963-120.
- [7] Alduse, B. P., Jung, S., and Vanli, O. A., "Condition-Based Updating of the Fragility for Roof Covers under High Winds," *Journal of Building Engineering*, v. 2, June 2015, pp. 36-43

- [8] LaFave, J. M., Gao, Z., Holder, D. E., Kuo, M. J., and Fahnestock, L. A., "Commercial and Residential Building Performance during the May 20, 2013, Tornado in Moore, Oklahoma," *ASCE Journal of Performance of Constructed Facilities*, v. 30, no. 2, April 2016
- [9] Ashutosh Sharma, Hemant Mittal, Ajay Gairola, Mitigation of wind load on tall buildings through aerodynamic modifications: Review, *Journal of Building Engineering*, Volume 18, 2018, Pages 180-194, <https://doi.org/10.1016/j.jobe.2018.03.005>
- [10] Aly, A.-M. and Bresowar, J., "Aerodynamic Mitigation of Wind-Induced Uplift Forces on Low-Rise Buildings: A Comparative Study," *Journal of Building Engineering*, v. 5, March 2016, pp. 267-276
- [11] X.J. Wang, Q.S. Li, B.W. Yan, J.C. Li, Field measurements of wind effects on a low-rise building with roof overhang during typhoons, *Journal of Wind Engineering and Industrial Aerodynamics*, Volume 176, 2018, Pages 143-157
- [12] Xiaowen Ji, Guoqing Huang, Xinxin Zhang, Gregory A. Kopp, Vulnerability analysis of steel roofing cladding: Influence of wind directionality, *Engineering Structures*, Volume 156, 2018, Pages 587-597
- [13] R.T. Ratay, An overview of forensic structural engineering, *Struct. Eng. Int.*, No. 3 (2017) 338-343.
- [14] EN 1991, Eurocode 1 — Actions on structures, CEN, Brussels, 2002.
- [15] STAAD.Pro V8i, Technical Reference Manual, Bentley Sustaining Infrastructure, 2012.
- [16] EN 1990, Eurocode — Basis of structural design, CEN, Brussels, 2002.
- [17] EN 1993-1-1, Eurocode 3 — Design of steel structures - Part 1-1: general rules and rules for buildings, CEN, Brussels, 2005.
- [18] EN 1998-1-1, Eurocode 8 — Design of structures for earthquake resistance - Part 1: general rules, seismic actions and rules for buildings, CEN, Brussels, 2003.
- [19] SOFiSTiK, Software Manuals, SOFiSTiK AG, www.sofistik.com, 2016.
- [20] Abaqus, v. 6.14, Analysis User's Manual, DS Simulia Corp., Online Documentation, 2015.
- [21] T. von Karman, Progress in the statistical theory of turbulence, *Proceedings of the National Academy of Sciences of the USA* (1948) 530-539.
- [22] Maraveas, C., Balokas, G. and Tsavdaridis, K.D. (2015) Numerical Evaluation on Shell Buckling of Empty Thin-Walled Steel Tanks Under Wind Load According to

Current American and European Design Codes. Thin-Walled Structures. 95, pp. 152-160.

- [23] Nikitas, N., Macdonald, J.H.G. and Tsavdaridis, K.D. (2014) Modal Analysis, Encyclopedia of Earthquake Engineering, Springer Verlag. pp. 1-22.
- [24] Tsavdaridis, K.D. (2014) Strengthening Techniques: Code-Deficient Steel Buildings, Encyclopedia of Earthquake Engineering, Springer Verlag. pp. 1-26.